Available online at www.sciencedirect.com
ScienceDirect
Trans. Nonferrous Met. Soc. China 32(2022) 2993−3004
Transactions of Nonferrous Metals Society of China
www.tnmsc.cn

Porous ceramic coating formed on 316L by laser cladding combined plasma electrolytic oxidation for biomedical application

Guo-long WU[1,2,3], Shuo ZHANG[1,2,3], Ye WANG[1,2,3], Min SUN[1,2,3],
Qun-li ZHANG[1,2,3], Volodymyr KOVALENKO[1,4], Jian-hua YAO[1,2,3]

1. College of Mechanical Engineering, Zhejiang University of Technology, Hangzhou 310014, China;
2. Institute of Laser Advanced Manufacturing, Zhejiang University of Technology, Hangzhou 310014, China;
3. Collaborative Innovation Center of High-end Laser Manufacturing Equipment, Zhejiang University of Technology, Hangzhou 310014, China;
4. Laser Technology Research Institute, National Technical University of Ukraine "Kiev Polytechnic Institute", Kiev, 03056, Ukraine

Received 19 August 2021; accepted 2 March 2022

Abstract: In order to improve the bioactivity of 316L stainless steel, a titanium layer was prepared on the surface of 316L by laser cladding (LC), followed by plasma electrolytic oxidation (PEO) to form a porous ceramic coating on titanium layer. The morphologies, microstructure and compositions of the coated samples were characterized by 3D surface profiler, SEM, EDS, XRD and XPS. The corrosion resistance and bioactivity of the coatings were evaluated by potentiodynamic polarization and immersion test in simulated body fluid (SBF), respectively. The results showed that the porous ceramic coating mainly consisted of anatase and rutile, and highly crystalline HA was also detected. The main elements of the PEO coating are Ca, P, Ti and O. The LC+PEO composite bio-coating has more excellent corrosion resistance than the 316L substrate in simulated body fluid. Furthermore, the composite coating could effectively improve the bioactivity of 316L stainless steel.

Key words: 316L stainless steel; laser cladding; titanium; plasma electrolytic oxidation; bioactivity

1 Introduction

316L stainless steel is widely used as biomaterials in medical field because of its ease of manufacturing, excellent mechanical property and cost effectiveness [1−3]. However, it is difficult for 316L stainless steel to form a real chemical bond with human bone tissue due to its low biocompatibility, low bioactivity and high modulus of elasticity [4]. Moreover, the corrosion and wear resistance of 316L stainless steel is poor in vivo environment. Some studies have shown that 316L stainless steel would release Cr^{3+} and Cr^{5+}, and diffuse to surrounding tissues, causing inflammation and necrosis of surrounding tissues, which ultimately leads to implantation failure due to corrosion and wear [5−7]. Therefore, surface treatment of 316L is one of the most effective solutions. At present, the surface modification technology of steel mainly includes thermal chemical reaction spraying, sol−gel, slurry, PVD, CVD and plasma spray [8−10]. However, the low bonding strength between the coating and the substrate, and the defects such as cracks in the coating are inevitable [11−13].

Plasma electrolytic oxidation (PEO) is a promising surface modification technology using

Corresponding author: Jian-hua YAO, Tel: +86-13735515066, E-mail: laser@zjut.edu.cn
DOI: 10.1016/S1003-6326(22)65998-3

the instantaneous high pressure and high temperature generated by micro-arc discharge to form porous ceramic oxide coating [14−16]. Due to its environmentally friendly characteristic and ability of metallurgical combination of the rough surface layer, it is especially suitable for biomedical applications of titanium alloys [17]. However, PEO is currently mainly applied to valve metals such as Al, Mg, Ti and their alloys. Laser cladding (LC) is a kind of laser surface modification technology which is metallurgically bonded with the substrate [18−20]. Titanium layer prepared by laser cladding on stainless steel makes its surface possess unique properties of titanium to a certain extent, such as good mechanical properties, low modulus of elasticity and corrosion resistance [21−24]. In order to improve the bioactivity, a porous titania coating containing Ca and P elements was formed by PEO using the LC titanium as a base layer, which further makes the titanium layer better bond with surrounding tissues in human environment. The surface of 316L medical stainless steel not only has excellent properties of titanium, but also can satisfy the clinic requirement that the surface of implant material has biology. Therefore, it is feasible that LC plus PEO were used to fabricate a composite porous ceramic bio-coating on 316L. The coating has high binding strength, good biological activity and corrosion resistance, which further improves the economic value and application prospect of 316L.

In our previous study, a Ca/P based ceramic coating was fabricated on TC4 titanium alloy which was produced by selective laser melting [25,26]. There is no study about formation, characterization and investigation of bioactivity of Ca/P based composite bio-coating on 316L by LC and PEO, although there are many studies about the Ca/P based coatings produced on the bulk titanium alloys [25−27]. In this study, LC and PEO hybrid techniques were combined to provide a double-layer (LC+PEO) coating system. The microstructure, thickness, and compositions of the composite coating were investigated. In addition, the surface properties of the samples were measured from the aspects of corrosion resistance and bioactivity. Growth characteristics through LC and PEO on 316L substrate was also discussed. This method effectively solves the technical defect that the ceramic coating of stainless steel cannot be prepared by PEO directly, and the results could provide a new idea for the future application of bio-ceramic coating on 316L.

2 Experimental

2.1 Materials

The substrate is 316 stainless steel plates with dimensions of 40 mm × 50 mm × 10 mm. All the substrates were polished mechanically with 400#, 800#, and 1200# SiC abrasive papers and then cleaned by ultrasonic in ethanol. The industrial pure titanium powder (99.7% purity) was used for the laser cladding process, as shown in Fig. 1.

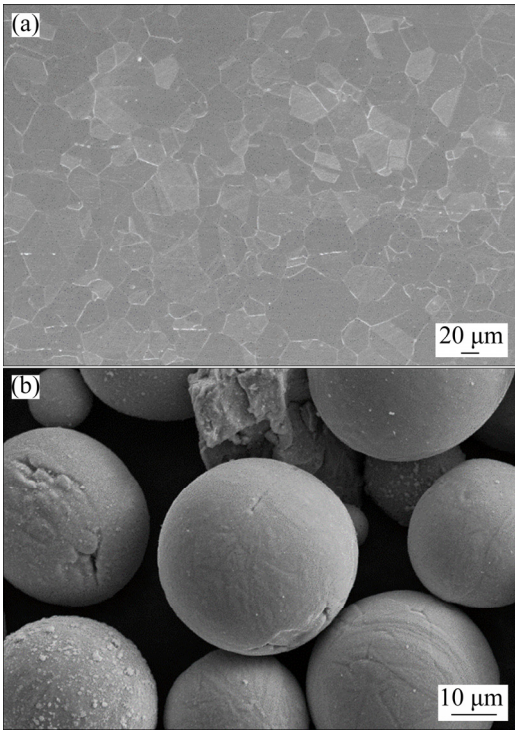

Fig. 1 Microstructure of 316L substrate (a) and morphologies of pure Ti powder (b)

2.2 Coating preparation

As illustrated in Fig. 2, the process consists of laser cladding in the pure titanium layer on the 316L substrate firstly, which will be coated by using the PEO process in a second step. LC layer was fabricated using SLM 125 HL machine with a 500 W fiber laser matched galvanometer scanning system, which was supplied by SLM Solutions GmbH, Germany. The optimal preparation process of pure titanium layer was the laser power of 400 W, scanning speed of 200 mm/s, laser spot size of 0.12 mm, scanning distance of 0.06 mm and layer

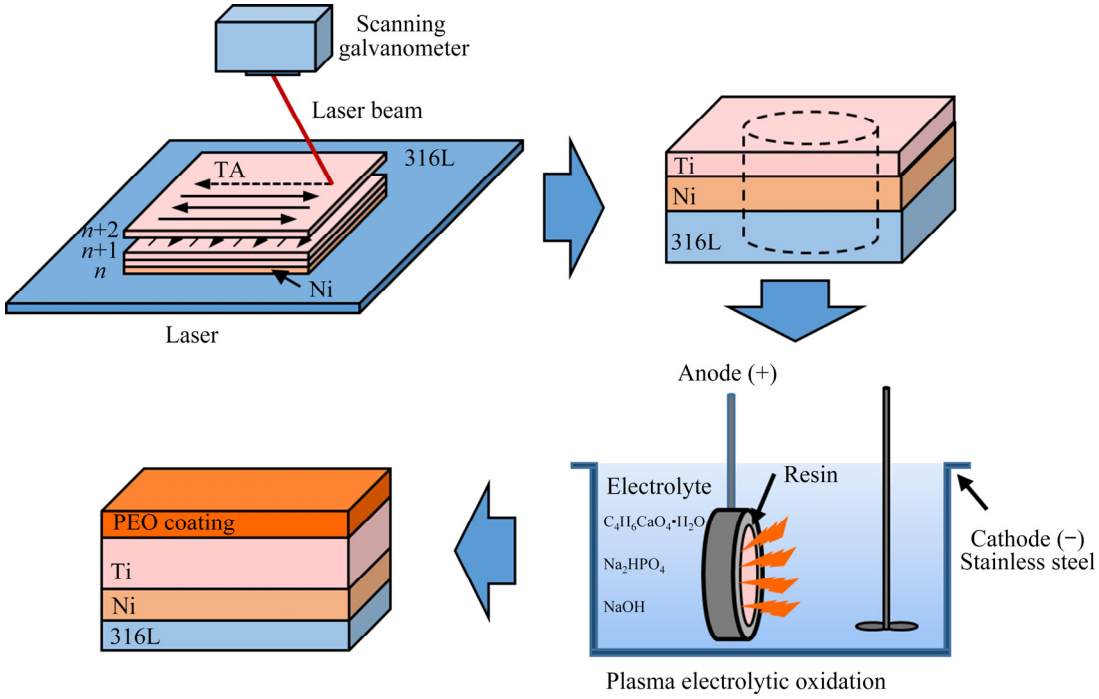

Fig. 2 Schematic description of duplex surface treatments performed on 316L steel by laser cladding (LC) combined plasma electrolytic oxidation (PEO)

thickness of 0.1 mm. In order to enhance the bonding strength between pure titanium layer and substrate, the transition layer of nickel with thickness of 300 μm was prepared on the surface of steel before laser cladding of titanium layer. Therefore, the optimized thickness of pure titanium layer with 400 μm was chosen to improve the quality of PEO coating according to the previous experiment.

After LC processing, the specimens were cut into *d* 15 mm × 5 mm by wire cutting. Then all surfaces except the titanium layer were sealed with epoxy resin and polyester, and then placed in an oven at 45 °C for 8 h. The PEO coating was formed on LC coated 316L. The LC coated 316L was used as the anode, and a stainless steel electrolyzer was used as the cathode during the PEO process. The electrolyte was an aqueous solution consisting of 0.1 mol/L $C_4H_6CaO_4 \cdot H_2O$ and 0.06 mol/L Na_2HPO_4, at the same time, NaOH was added to the electrolyte to adjust the pH of the solution to 12−13. The optimal electrical parameters of PEO were set as current density of 9 A/dm^2, duty cycle of 20% and pulse frequency of 500 Hz. After PEO treatment, the samples were washed for 60 s with distilled water and then disinfected by ultrasonication for 30 s in 70% ethanol, 5 min immersion in demineralized water, and 30 s ultrasonication in demineralized water.

2.3 Coating characterization

The surface and cross-section morphology of the LC and LC+PEO coatings were examined by scanning electron microscopy (SEM, ΣIGMA, ZEISS). The surface morphology and roughness of the prepared samples were measured by 3D surface profiler (SuperView W1, China) based on scanning white light interferometry. Energy dispersive X-ray spectroscopy (EDS) in connection with the SEM system and X-ray photoelectron spectroscopy (XPS, Kratos-Axis Ultra spectrometer) were used to analyze the elemental compositions of the coatings. The phase structure of the coatings was carried out by using X-ray diffractometer (XRD, X' Pert PRO, PNAlytical).

2.4 Electrochemical test

The corrosion behavior of LC and LC+PEO coatings were evaluated by potentiodynamic polarization tests on an electrochemical workstation (CHI660E, Shanghai, China) in 36.5 °C SBF solution, which was a three-electrode cell with platinum as counter electrode, the sample surface was exposed to a test area of 1 cm^2 and electrode

saturated calomel electrode (SCE) as reference electrode. The potentiodynamic polarization test was performed at the sweep rate of 0.5 mV/s in simulate body fluid (SBF) at 36.5 °C. Each group was tested in parallel 3 times. The chemical composition of SBF solution described by KOKUBO [28] is shown in Table 1. The solution was prepared from analytically deionized water and pure chemicals. All the samples were immersed in SBF solution for 60 min before the open circuit potential (OCP) were tested.

2.5 Bioactivity test

KOKUBO [28] found that the formation of bone-like apatite on the surface of artificial materials directly reflects the bonding with living bone. The chemical composition and structure of apatite is similar to that of natural bone minerals implanted in living organisms. Immersing the sample in a simulated body fluid (SBF) with the ion concentration almost equal to human plasma (Table 2), the formation of apatite can be replicated in vivo, thus demonstrating the biological activity of material. Many researchers consider this bioactivity assay to be very convenient and effective. In this study, each sample was placed in a plastic bottle containing 50 mL of SBF solution and stored in a constant temperature water at 36.5 °C. The solution was changed every 24 h. After soaking for 3 d, the samples were removed from the SBF, cleaned and dried in an air-dry closet. The dried samples were coated with gold and analyzed by SEM and EDS to study bioactivity (nucleation and growth of apatite) of the surface.

3 Results and discussion

3.1 Microscopic characteristics of LC layer

Figure 3 presents the EDS spectra of the cross section of the laser cladding layer. It can be seen that Ti mainly exists in the cladding layer, and a small amount of Ti element is diluted in the Ti−Ni transition layer during laser cladding. As the nickel layer is an intermediate coating between the substrate and titanium layer, there is element dilution during the LC process. Therefore, Ni has more intermediate distribution and less upper and lower distribution. Fe mainly occurs in 316L stainless steel matrix, and its distribution in nickel coating and titanium coating decreases gradually. At the top of the LC coating, Ti is the main component element, and there are almost no Fe and Ni. The microstructure of LC titanium layer is presented in Fig. 4. The top part (Area *A* in Fig. 4) of the sample was composed of coarse and irregular light grey dendrites, with a thick boundary phase in-between, which was a mixture of the light and dark phases. It is mainly non-equilibrium α' titanium. The light grey dendrites corresponded to the NiTi phase [29]. For the middle sample, a dendritic pattern, with preferred growth direction, was readily observable. Furthermore, the NiTi dendritic structure showed a random orientation at the top of the LC coating while the central area of the cladding layer seems to be preferentially oriented. It is well-accepted that the direction of the maximum thermal gradient can directly affect the growth direction of dendrite crystals [30]. The higher the maximal thermal gradient is, the more oriented the dendrite structure will be. However, the top of the coating diffused a large amount of heat into the air in the atmospheric environment and resulted in a significant heat loss, thus, the reduced thermal gradient in the top region resulted in more random orientation of the dendrite structure.

3.2 Microstructural characteristics of bio-coating

The microstructural characteristics of the LC+PEO coatings was investigated by 3D surface

Table 1 Chemical composition of SBF solution (g/L)

NaCl	$NaHCO_3$	KCl	$K_2HPO_4·3H_2O$	$MgCl_2·6H_2O$	$CaCl_2$	Na_2SO_4	Tris
8.035	0.355	0.225	0.231	0.311	0.292	0.072	6.118

Table 2 Ion concentrations of SBF, in comparison with those of human blood plasma (mmol/L)

Solution	Na^+	K^+	Mg^+	Ca^+	Cl^-	HCO_3^-	HPO_4^{2-}	SO_4^{2-}
Human body	142	5.0	1.5	2.5	103.0	27.0	1.0	0.5
SBF	142	5.0	1.5	2.5	147.8	4.2	1.0	0.5

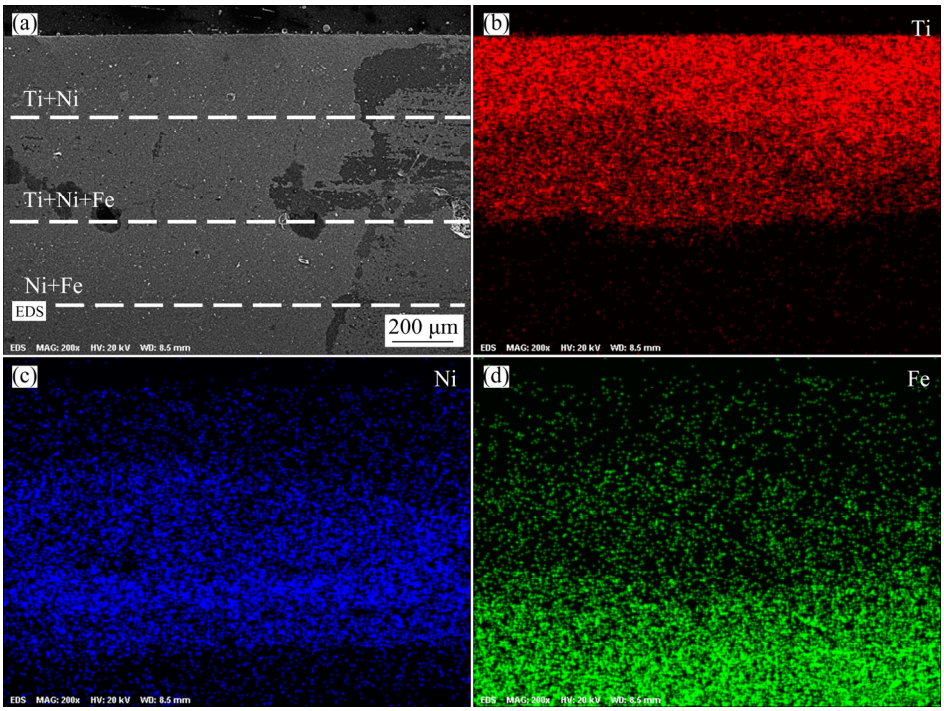

Fig. 3 EDS results of cross section of LC layer: (a) Scanning area; (b) Ti; (c) Ni; (d) Fe

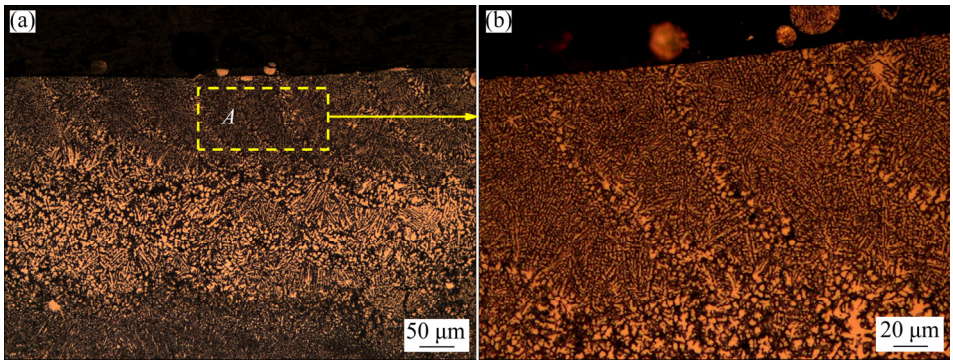

Fig. 4 Microstructure of LC titanium layer

profiler, and SEM image is exhibited in Fig. 5. The results indicate that the initial LC tracks are no longer visible, but the surface of the coating exhibits the highest surface roughness, as shown in Fig. 5(a). Though there are many similar craters, there are a little different from the traditional PEO coating on titanium [25,26]. The S_a (arithmetic mean deviation) and S_q (root mean square deviation) of LC+PEO coating are 1.195 and 1.600, respectively. Figures 5(a, b) show the typical morphology of the PEO coating, displaying volcano-like structures with randomly distributed micro-pores. Two types of discharges in the process of micro-arc oxidation are found: (1) surface discharges with relatively weak strength are formed by the bursting of gas envelope; (2) penetrating discharges due to the breakdown of the oxide coating with strong intensity [31]. The evolution of the porous surface morphology of the PEO coatings shows that the surface discharge is dominant during the PEO process. According to previous study, the pores and cracks of PEO coating provide channels for the corrosion medium, accelerating corrosion process. Therefore, the surface porosity of coating was analyzed by Image J. The results present that the size of many micro-pores is smaller than 0.5 μm, and the porosity of the PEO coating is 4.31%.

The corrosion resistance of the PEO coating formed on the titanium mainly depends on its ability to resist the migration of corrosive ions to the substrate/coating interface and the movement of metal ions away from the substrate surface, which

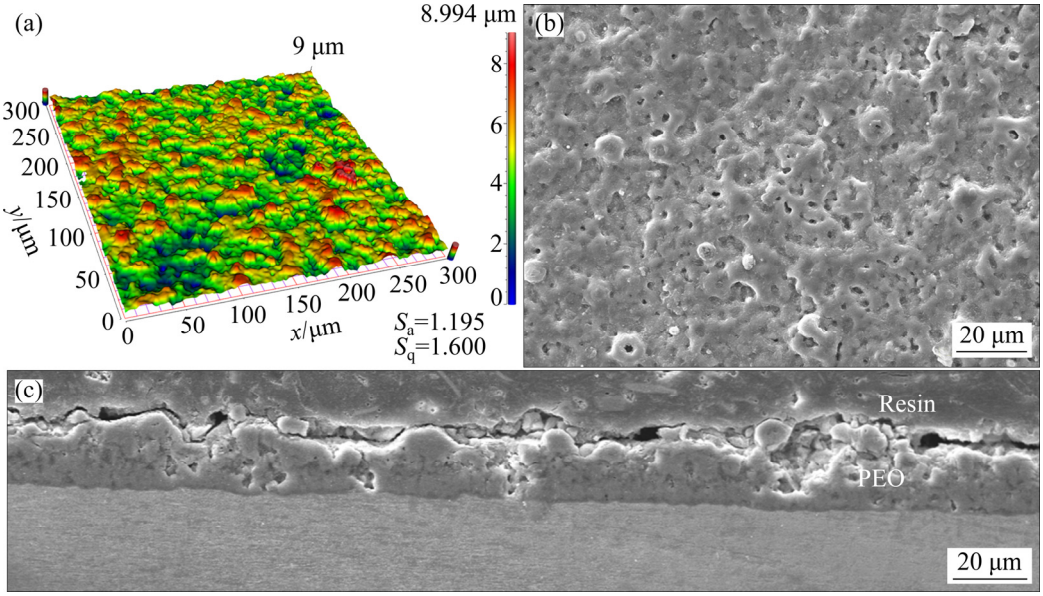

Fig. 5 Microstructural characteristics of LC+PEO coatings: (a) Surface roughness; (b) Surface morphology; (c) Cross-section thickness

in turn is mostly decided by the morphology, structure and barrier coating features of the coating [32]. Reducing the porosity and defects will effectively improve the anti-corrosion performance of the PEO coating. Besides, the thickness also decides the protection effect of PEO coating in the condition of long-term corrosion. As shown in Fig. 5(c), the PEO coating uniformly distributes on the LC titanium layer, and its thickness is about 35 μm. The sawtooth metallurgical bond is formed between the ceramic coating and the substrate, and the interface is well combined. Similarity with other reports, the coating is divided into a two-layer structure of an inner dense layer and outer loose layer [33]. It can be seen that the outer loose layer of coating is considerably dense, which results in the corrosive penetrates the porous layer difficultly through the micropores and then reacting with the inner compact layer [34].

3.3 Chemical compositions of bio-coating

The EDS result of the surface composition and element distribution of the PEO coating is shown in Fig. 6. The surface element composition of the PEO coating on the LC titanium layer is characterized by Ti, O, Ca, P, Ni and Fe (Fig. 6(a)). The element characteristics of Ti and O indicate the presence of TiO_2 in the PEO coating. Increasing the contents of bioactive elements in PEO coating is advantageous to enhance the bioactivity performance of coating. Ca and P incorporated into the oxide layer are likely to have originated from the electrolyte, and their contents are 11.96 and 6.93 at.%, respectively. At the same time, there are small amounts of Ni in the PEO coating. It can be clearly seen that the elements of the cladding layer gradually diffuse into the composite coating, which enhances the bonding strength between the two coatings. As shown in Fig. 6(b), the distribution curve of the six elements was gentle and the element content did not change noticeably. At the interface between the unoxidized titanium coating and the PEO ceramic coating, the Fe contents decreased to 0, and O, Ca, Ni and P presented. The rapid increase in the content of Ca and P elements demonstrates that Ca and P elements mainly exist on the surface of the PEO coating. Furthermore, as the distance from the interface increases, the Ti element first decreases sharply and then remains stable, whereas the O element first increases and then remains stable. As there was no diffusion layer between the ceramic and the cladding titanium layers, there was no significant gradient change in the elemental content. Compared with the cladding zone, the contents of Ti and O in the PEO coating are much more. On the contrary, there are small amounts of Ni in the PEO coating. The results reveal that the diffusion of the elements of the cladding coating into the composite coating leads to the enhancement of the interfacial bonding ability of the two coatings.

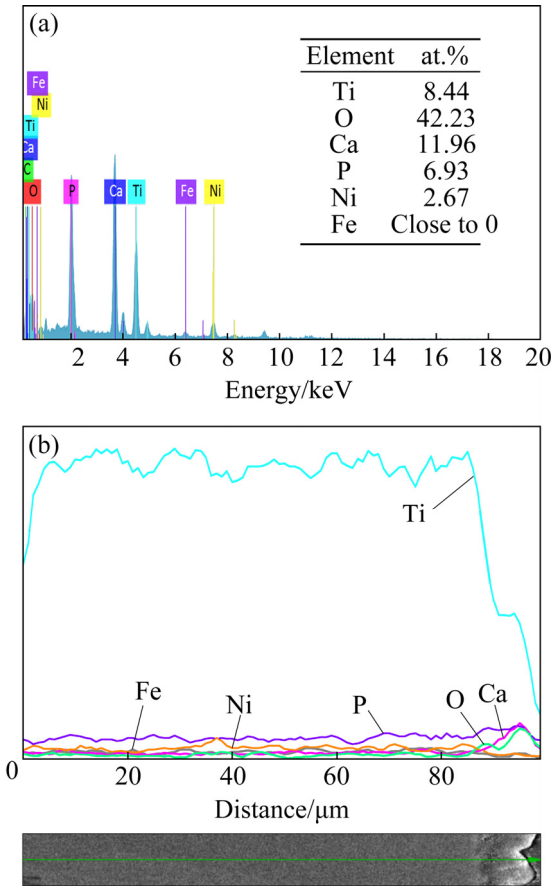

Fig. 6 Surface element composition and element distribution in cross-section of PEO coating observed by EDS: (a) Surface element composition; (b) EDS line scanning

Figure 7 shows the XRD patterns of the LC titanium coating and LC+PEO coating on the 316L. The main phases of the LC coating are composed of Ti and TiNi, and no oxides were detected. The main phases of the LC+PEO coating consisted of rutile, anatase and HA. In addition, the NiTi diffraction peak from LC coating disappears because of the enough thickness of the PEO coating to prevent the X-ray from penetrating it. In general, the TiO_2-phase mainly presents in three crystalline polymorphs of the brookite, anatase and rutile, among which the anatase phase is metastable and transfers to the rutile-phase above 800 °C [35]. It can be seen that the enhanced electric arc phenomenon in the PEO process accelerates the transformation of anatase to rutile phase. Due to better corrosion resistance of the rutile-phase, anatase-phase gradually became a research focus in the field of surface science [36,37]. It is clear that the intensity of the anatase (101) plane is lower than

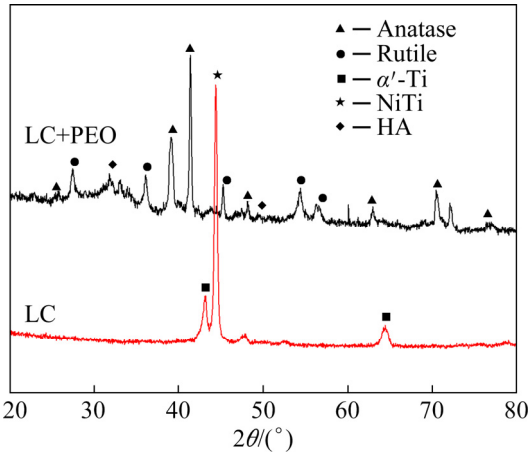

Fig. 7 XRD patters of titanium coating formed by laser cladding on 316L stainless steel before and after PEO

that of the rutile (110) plane, as shown in Fig. 7. This indicates that more rutile phases form in the LC+PEO coating.

The chemical state of Ti, O, P and Ca elements in the PEO coating on cladding titanium coating was analyzed by the high-resolution XPS. As shown in Fig. 8, The Ti $2p_{3/2}$ and Ti $2p_{1/2}$ XPS peaks of the coating, located at 458.63 and 464.34 eV, respectively, are well fitted to those of Ti 2p in TiO_2 [38]. The P 2p peaks are at the binding energy of 133.02 and 133.85 eV, which separately correspond to PO_4^{3-} and HA [10]. The Ca 2p peak exhibited doublet spectra of Ca $2p_{3/2}$ and Ca $2p_{1/2}$. The high energy of Ca $2p_{1/2}$ is located at 350.88 eV, while the low energy of Ca $2p_{3/2}$ exhibited two peaks at 347.47 and 346.87 eV, corresponding to Ca 2p in HA, $Ca_3(PO_4)_2$ and CaO respectively [10,39]. Depending on the results of EDS, XRD and XPS, the electrochemical reactions in the PEO process can be described as follows:

$$Ti-4e \rightarrow Ti^{4+} \quad (1)$$

$$2H_2O+2e \rightarrow H_2+2OH^- \quad (2)$$

$$Ti^{4+}+4OH^- \rightarrow TiO_2+2H_2O \quad (3)$$

$$Ca(CH_3COO)_2 \rightarrow Ca^{2+}+2CH_3COO^- \quad (4)$$

$$Na_2HPO_4 \rightarrow 2Na^+ + HPO_4^{2-} \quad (5)$$

$$Ca^{2+}+HPO_4^{2-} \rightarrow CaHPO_4 \quad (6)$$

$$3CaHPO_4 \rightarrow Ca_3(PO_4)_2+PO_4^{3-}+2H^+ \quad (7)$$

$$10Ca^{2+}+6PO_4^{2-}+2OH^- \rightarrow Ca_{10}(PO_4)_6(OH)_2 \quad (8)$$

$$3Ca^{2+}+2PO_4^{2-} \rightarrow Ca_3(PO_4)_2 \quad (9)$$

$$Ca(OH)_2 \rightarrow CaO+H_2O \quad (10)$$

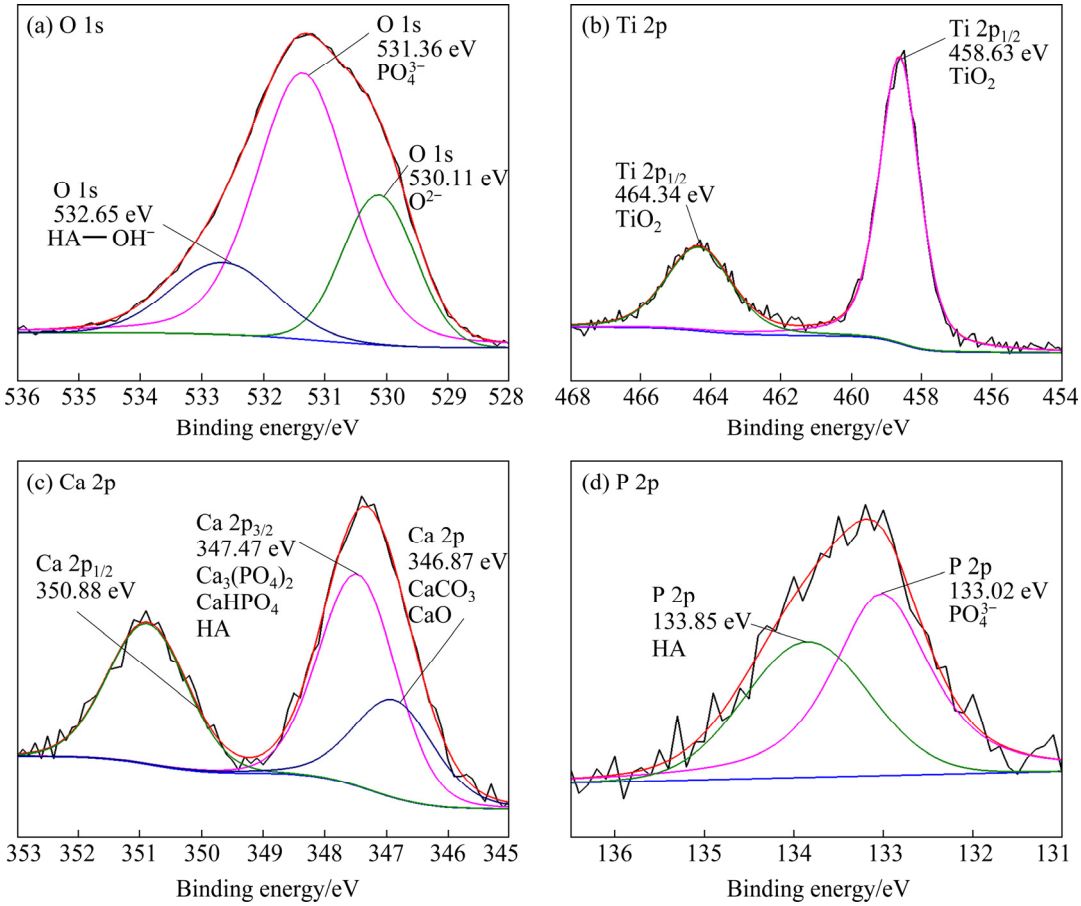

Fig. 8 High-resolution XPS spectra of O 1s, Ti 2p, Ca 2p and P 2p of LC+PEO coating

3.4 Corrosion resistance

The potentiodynamic polarization curves of 316L, LC titanium coating and LC+PEO coating in SBF solution at 36.5 °C are shown in Fig. 9. Table 3 shows the corrosion potential (φ_{corr}) and corrosion current density (J_{corr}) of the three samples. It can be seen from Table 3 that the corrosion potentials of the 316L substrate and LC titanium coating are (−308.5±3.0) and (−311.6±3.1) mV respectively, which are lower than the LC+PEO coating, about (−186.8±1.8) mV. The more positive the potential, the higher the chemical stability of the sample in a corrosive environment. Corrosion potential is shifted towards a noble direction by 125 mV, indicating that the LC+PEO coating provides the excellent corrosion protection for the substrate.

The corrosion current density (J_{corr}) is used as the critical parameter to evaluate the reaction kinetics of corrosion further. The J_{corr} values of the LC titanium coating and LC+PEO coating are 4.021×10^{-7} and 1.615×10^{-7} A/cm^2, respectively, which are much lower than that of the 316L substrate. The corrosion current density decreases by

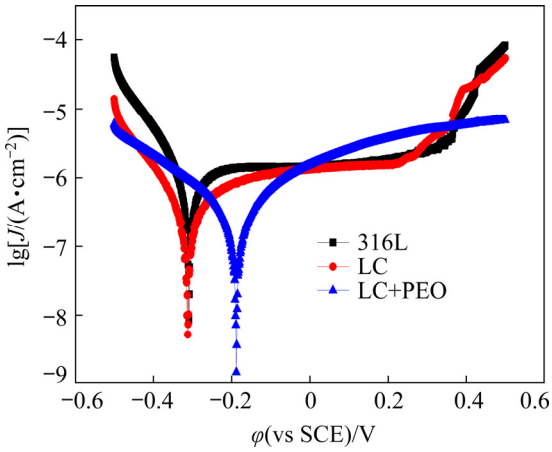

Fig. 9 Polarization curves of 316L, LC titanium coating and LC+PEO coating in SBF solution at 36.5 °C

Table 3 Results of potentiodynamic polarization curves of 316L, LC titanium coating and LC+PEO coating in SBF solution at 36.5 °C

Sample	φ_{corr}(vs SCE)/mV	J_{corr}/(A·cm^{-2})
316L	−308.5±3.0	1.194×10^{-6}
LC	−311.6±3.1	4.021×10^{-7}
LC+PEO	−186.8±1.8	1.615×10^{-7}

approximately one order, with respect to the 316L substrate. In summary, the LC+PEO coating significantly improves the corrosion resistance of 316L.

3.5 Bioactivity

In order to compare the bioactivity of 316L, LC and LC+PEO coating, the three samples were immersed in SBF of pH 7.4 at 36.5 °C for 3 d. Figure 10 shows the surface morphologies of 316L, LC and LC+ PEO coating after immersion. It can be clearly found that a bony apatite layer of small crystal size is formed on the surface of the LC titanium and LC+PEO coatings after immersion. In contrast, there is almost no apatite formed on the 316L substrate. Thus, it can be seen from the formation result that the bioactivity of 316L substrate is found to be poor. In general, the size of apatite crystals formed on the LC+PEO coating is significantly larger than that on the LC. Table 4 shows the contents of Ca and P on the surface of the samples after immersion. The low Ca/P molar ratio on the surface of LC coating indicates that its biological activity is poor, while the Ca/P molar ratio on the surface of LC+PEO coating is 1.76, which closes to the theoretical ratio of 1.67 of HA. The bioactivity of 316L substrate is clearly enhanced due to the LC+PEO coating. This is mainly because there are a lot of micro-pores on the surface of the LC+PEO coating. On the one hand, the micro-pores provide nucleation sites for the formation of apatite. The solution flows and diffuses slowly in the local area of the micropores, so the nucleation threshold can be reached quickly. On the other hand, the PEO treatment can effectively improve the bioactivity of the titanium coating due to the Ca and P after PEO treatment. It is found that the ability to form HA on the surface of a biomaterial indirectly reflects its potential to bind to bone tissue. The formation of stoichiometric HA from the calcium, phosphate and hydroxyl ions can be expressed as Eq. (8). The formation process of HA crystals on the oxide film is affected by two factors: nucleation of HA and diffusion of Ca and P ions from the inner layer towards the film surface. The increase in the growth rate of the apatite layer with increasing contents of HA and α-$Ca_3(PO_4)_2$ and composition of Ca and P ions can be attributed to the following reasons [10]: (1) an increase in the localized initial supersaturation of the SBF with respect to apatite as more sites for HA dissolution is available; (2) a decrease in the incubation time needed for the initial supersaturation is achieved.

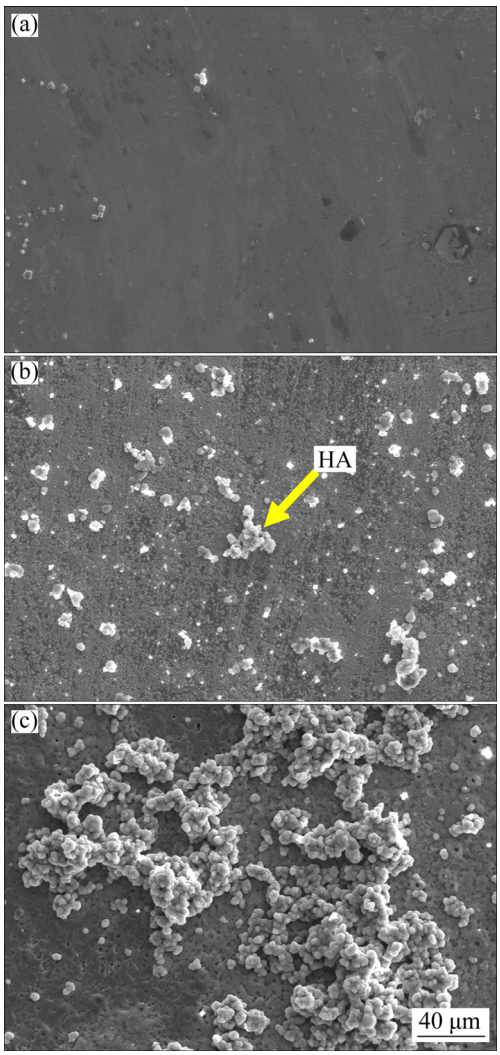

Fig. 10 SEM images showing surface morphologies of 316L (a), LC (b) and LC+PEO coating (c) after immersion in SBF for 3 d

Table 4 Contents of Ca and P on surface of samples after immersion in SBF for 3 d

Sample	Ca content/at.%	P content/at.%	Ca/P ratio
316L	–	–	–
LC	2.6	4.8	0.54
LC+PEO	16.35	9.29	1.76

4 Conclusions

(1) The surface of the LC+PEO coating has porous characteristics. After LC+PEO processes, the Ca, P and O required for the formation of HA

are uniformly distributed on the entire surface. The main phases of the LC+PEO coating are composed of rutile, anatase and HA.

(2) The LC+PEO coating remarkably improves the corrosion resistance of 316L. The surface morphology and phase structure of LC+PEO have a positive effect on the formation of secondary apatite structure in SBF.

(3) The uniform distribution of Ca, P and O elements required to form the secondary apatite structure is observed on the whole surface after immersion in SBF. The LC+PEO composite technology makes the 316L implant surface modify with bioactivity and biocompatibility, which will become a promising surface modification technology.

Acknowledgments

The authors would like to appreciate financial support from the National Natural Science Foundation of China (No. 51975533), National Safety Academic Fund, China (No. U2130122), and Public Projects of Zhejiang Province, China (Nos. LGJ22E050002, LGJ20E050002).

References

[1] ZHOU Hua-juan, JIANG Meng, XIN Yun-chuan, SUN Guang-yao, LONG Shi-wei, BAO Shan-hu, CAO Xun, JI Shi-dong, JIN Ping. Surface deposition of graphene layer for bioactivity improvement of biomedical 316 stainless steel [J]. Materials Letters, 2017, 192:123−127.

[2] KALIARAJ G S, VISHWAKARMA V, KIRUBAHARAN A M K. Biocompatible Zirconia-Coated 316 stainless steel with anticorrosive behavior for biomedical application [J]. Ceramics International, 2018, 44: 9780−9786.

[3] LODHI M J K, DEEN K M, GREENLEE-WACKER M C, HAIDER W. Additively manufactured 316L stainless steel with improved corrosion resistance and biological response for biomedical applications [J]. Additive Manufacturing, 2019, 27: 8−19.

[4] YANG Zhi-lu, TU Qiu-fen, MAITZ M F, ZHOU Shuo, WANG Jin, HUANG Nan. Direct thrombin inhibitor-bivalirudin functionalized plasma polymerized allylamine coating for improved biocompatibility of vascular devices [J]. Biomaterials, 2012, 33: 7959−7971.

[5] KATTA P, NALLIYAN R. Corrosion resistance with self-healing behavior and biocompatibility of Ce incorporated niobium oxide coated 316L SS for orthopedic applications [J]. Surface and Coatings Technology, 2019, 375: 715−726.

[6] YETIM A F, YAZıC1 M. Wear resistance and non-magnetic layer formation on 316L implant material with plasma nitriding [J]. Journal of Bionic Engineering, 2014, 11: 620−629.

[7] GARCIA-LOBATO M A, MTZ-ENRIQUEZ A I, GARCIA C R, VELAZQUEZ-MANZANARES M, AVALOS-BELMONTES F, RAMOS-GONZALEZ R, GARCIA-CERDA L A. Corrosion resistance and in vitro bioactivity of dense and porous titania coatings deposited on 316L SS by spraying method [J]. Applied Surface Science, 2019, 484: 975−980.

[8] MOSHREF-JAVADI M, EDRIS H, SHAFYEI A, SALIMI-JAZI H, ABDOLVAND E. Evaluation of hydrogen permeation through standalone thermally sprayed coatings of AISI 316L stainless steel [J]. International Journal of Hydrogen Energy, 2018, 43: 4657−4670.

[9] ZHANG Ke-dong, DENG Jian-xin, LEI Shu-ting,YU Xiao-ming. Effect of micro/nano-textures and burnished MoS_2 addition on the tribological properties of PVD TiAlN coatings against AISI 316 stainless steel [J]. Surface and Coatings Technology, 2016, 291: 382−395.

[10] GUO Shu-wei, XU Dong-hai, LIANG Yu, GONG Yan-meng, LI Yan-hui. Corrosion characterization of ZrO_2 and TiO_2 ceramic coatings via air plasma spraying on 316 stainless steel in oxygenated sub- and supercritical water [J]. The Journal of Supercritical Fluids, 2020, 157: 104716.

[11] SINGH H, KUMAR R, PRAKASH C, SINGH S. HA-based coating by plasma spray techniques on titanium alloy for orthopedic applications [J]. Materials Today Proceedings, 2022, 50: 612−628.

[12] SARGIN F, ERDOGAN G, KANBUR K, TURK A. Investigation of in vitro behavior of plasma sprayed Ti, TiO_2 and HA coatings on PEEK [J]. Surface and Coatings Technology, 2021, 411: 126965.

[13] KUMARI R, MAJUMDAR J D. Microstructure and surface mechanical properties of plasma spray deposited and post spray heat treated hydroxyapatite (HA) based composite coating on titanium alloy (Ti−6Al−4V) substrate [J]. Materials Characterization, 2017, 131: 12−20.

[14] WANG Ye, LU Dan-hua, WU Guo-long, CHEN Kai-ye, WU Hao, ZHANG Qun-li, YAO Jian-hua. Effect of laser surface remelting pretreatment with different energy density on MAO bioceramic coating [J]. Surface and Coatings Technology, 2020, 393: 125815.

[15] KRZĄKAŁA A, KAZEK-KEŚIK A, SIMKA W. Application of plasma electrolytic oxidation to bioactive surface formation on titanium and its alloys [J]. RSC Advances, 2013, 3: 19725.

[16] YAO Z Q, IVANISENKO Y, DIEMANT T, CARON A, CHUVILIN A, JIANG J Z, VALIEV R Z, QI M, FECHT H J. Synthesis and properties of hydroxyapatite-containing porous titania coating on ultrafine-grained titanium by micro-arc oxidation [J]. Acta Biomaterialia, 2010, 6: 2816−2825.

[17] XIU Peng, JIA Zhao-jun, LV Jia, YIN Chuan, CHENG Yan, ZHANG Ke, SONG Chun-li, LENG Hui-Jie, ZHENG Yu-feng, CAI Hong, LIU Zhong-jun. Tailored surface treatment of 3D printed porous Ti6Al4V by microarc oxidation for enhanced osseointegration via optimized bone in-growth patterns and interlocked bone/implant interface [J]. ACS Applied Materials & Interfaces, 2016, 8: 17964−17975.

[18] ZENG Ming, YAN Hong, YU Bao-biao, HU Zhi. Microstructure, microhardness and corrosion resistance of

laser cladding Ni-WC coating on AlSi5Cu1Mg alloy [J]. Transactions of Nonferrous Metals Society of China, 2021, 31: 2716−2728.

[19] LIU Jian-li, YU Hui-jun, CHEN Chuan-zhong, WENG Fei, DAI Jing-jie. Research and development status of laser cladding on magnesium alloys: A review [J]. Optics and Lasers in Engineering, 2017, 93: 195−210.

[20] KOVALEV O B, BEDENKO D V, ZAITSEV A V. Development and application of laser cladding modeling technique: From coaxial powder feeding to surface deposition and bead formation [J]. Applied Mathematical Modelling, 2018, 57: 339−359.

[21] GOGHERI M S,KASIRI-ASGARANI M, BAKHSHESHI-RAD H R,GHAYOUR H,RAFIEI M. Mechanical properties, corrosion behavior and biocompatibility of orthopedic pure titanium−magnesium alloy screw prepared by friction welding [J]. Transactions of Nonferrous Metals Society of China, 2020, 30(11): 2952−2966.

[22] WU Guo-long, WANG Ye, LIU Jian-hua, YAO Jian-hua. Influence of the Ti alloy substrate on the anodic oxidation in an environmentally-friendly electrolyte [J]. Surface and Coatings Technology, 2018, 344: 680−688.

[23] BIASETTO L, BERTOLINI R, ELSAYED H, GHIOTTI A, BRUSCHI S. Use of cryogenic machining to improve the adhesion of sphene bioceramic coatings on titanium substrates for dental and orthopaedic applications [J]. Ceramics International, 2019, 45: 5941−5951.

[24] ZHOU Rui, WEI Da-qing, CHENG Su, LI Bao-qiang, WANG Ya-ming, JIA De-chang, ZHOU Yu, GUO Hai-feng. The structure and in vitro apatite formation ability of porous titanium covered bioactive microarc oxidized TiO_2-based coatings containing Si, Na and Ca [J].Ceramics International, 2014, 40: 501−509.

[25] YAO Jian-hua, WANG Ye, WU Guo-long, SUN Min, WANG Miao, ZHANG Qun-li. Growth characteristics and properties of micro-arc oxidation coating on SLM-produced TC4 alloy for biomedical applications [J]. Applied Surface Science, 2019, 479: 727−737.

[26] WU Guo-long, WANG Ye, SUN Min, ZHANG Qun-li, YAO Jian-hua. Influence of microstructure of TC4 substrate on the MAO coating [J]. Surface Engineering, 2020, 36: 827−836.

[27] WANG Ying-jun, WANG Lin, ZHENG Hua-de, DU Chang, NING Cheng-yun, SHI Zhi-feng, XU Cai-xia, Effect of frequency on the structure and cell response of Ca- and P-containing MAO films [J]. Applied Surface Science, 2010, 256: 2018−2024.

[28] KOKUBO T. Bioactive glass ceramics: properties and applications [J]. Biomaterials, 1991, 12: 155−163.

[29] WANG Jun, PAN Zeng-xi, WANG Long, SU Li-hong, CARPENTER K, WANG Jian-sheng, WANG Rui-chao, LI Hui-jun. In-situ dual wire arc additive manufacturing of NiTi-coating on Ti6Al4V alloys: Microstructure characterization and mechanical properties [J]. Surface and Coatings Technology, 2020, 386: 125439.

[30] THIJS L, MONTERO SISTIAGA M L, WAUTHLE R, XIE Q G, KRUTH J P, van HUMBEECK J, Strong morphological and crystallographic texture and resulting yield strength anisotropy in selective laser melted tantalum [J]. Acta Materialia, 2013, 61: 4657−4668.

[31] HUSSEIN R O, NIE X, NORTHWOOD D O. An investigation of ceramic coating growth mechanisms in plasma electrolytic oxidation (PEO) processing [J]. Electrochimica Acta, 2013, 112: 111−119.

[32] AN Ling-yun, MA Ying, YAN Xiao-xu, WANG Sheng, WANG Zhan-ying. Effects of electrical parameters and their interactions on plasma electrolytic oxidation coatings on aluminum substrates [J]. Transactions of Nonferrous Metals Society of China, 2020, 30(4): 883−895.

[33] LIANG J, SRINIVASAN P B, BLAWERT C, DIETZEL W. Comparison of electrochemical corrosion behaviour of MgO and ZrO_2 coatings on AM50 magnesium alloy formed by plasma electrolytic oxidation [J]. Corrosion Science, 2009, 51: 2483−2492.

[34] DU Ke-qin, GUO Xing-hua, GUO Quan-zhong, WANG Yong, WANG Fu-hui, TIAN Ying. Effect of PEO coating microstructure on corrosion of Al 2024 [J]. Journal of the Electrochemical Society, 2012, 159: C597−C606.

[35] ZHAI Da-jun, FENG Ke-qin. Preparation of micro/nano-structured ceramic coatings on Ti6Al4V alloy by plasma electrolytic oxidation process [J]. Transactions of Nonferrous Metals Society of China, 2019, 29: 2546−2555.

[36] SHAO Hong-hong, YU Chun-Hang, XU Xiao-jing, WANG Ji, ZHAI Rui, WANG Xiao-jing. Influence of Ti nanocrystallization on microstructure, interface bonding, surface energy and blood compatibility of surface TiO_2 films [J]. Applied Surface Science, 2010, 257: 1649−1654.

[37] VIANA M M, SOARES V F, MOHALLEM N D S. Synthesis and characterization of TiO_2 nanoparticles [J]. Ceramics International, 2010, 36: 2047−2053.

[38] FRAUCHIGER V M, SCHLOTTIG F, GASSER B, TEXTOR M. Anodic plasma-chemical treatment of CP titanium surfaces for biomedical applications [J]. Biomaterials, 2004, 25: 593−606.

[39] HAN Yong, SUN Ji-feng, HUANG Xin. Formation mechanism of HA based coatings by micro-arc oxidation [J]. Electrochemistry Communications, 2008, 10: 510−513.

316L 表面激光熔覆复合等离子体电解氧化制备多孔陶瓷涂层及其生物应用

吴国龙[1,2,3]，张 烁[1,2,3]，王 晔[1,2,3]，孙 敏[1,2,3]，张群莉[1,2,3]，Volodymyr KOVALENKO[1,4]，姚建华[1,2,3]

1. 浙江工业大学 机械工程学院，杭州 310014；
2. 浙江工业大学 激光先进制造研究院，杭州 310014；
3. 浙江工业大学 高端激光制造设备协同创新中心，杭州 310014；
4. Laser Technology Research Institute, National Technical University of Ukraine “Kiev Polytechnic Institute”, Kiev, 03056, Ukraine

摘 要：为了提高 316L 不锈钢的生物活性，采用激光熔覆(LC)技术在 316L 不锈钢表面制备钛层，然后利用等离子体电解氧化(PEO)技术在钛层上形成多孔陶瓷涂层。采用三维表面轮廓仪、SEM、EDS、XRD 和 XPS 等测试方法对涂层试样的形貌、微观结构和组成进行表征。通过动电位极化曲线和模拟体液(SBF)浸泡试验，分别对涂层的耐腐蚀性和生物活性进行评价。结果表明，多孔陶瓷涂层主要由锐钛矿和金红石组成，并检测到高结晶 HA。陶瓷涂层的主要元素为 Ca、P、Ti 和 O。在模拟体液中，LC+PEO 复合生物涂层比 316L 基质具有更优异的耐腐蚀性，并且复合涂层能有效提高 316L 不锈钢的生物活性。

关键词：316L 不锈钢；激光熔覆；钛；等离子体电解氧化；生物活性

(Edited by Xiang-qun LI)